Research

Authors for correspondence:
Liu Qiuping
e-mail: liuqiuping@zjut.edu.cn
He Yuehui
e-mail: yuehui@csu.edu.cn

THE ROYAL SOCIETY PUBLISHING

Preparation of nanoporous BiVO$_4$/TiO$_2$/Ti film through electrodeposition for photoelectrochemical water splitting

Dong Hongxing[1], Liu Qiuping[2] and He Yuehui[3]

[1]College of Electromechanical Engineering, Hangzhou Polytechnic, Hangzhou, Zhejiang, People's Republic of China
[2]College of Chemical Engineering, Zhejiang University of Technology, Hangzhou, Zhejiang, People's Republic of China
[3]State Key Laboratory of Powder Metallurgy, Central South University, Changsha 410083, People's Republic of China

A nanoporous BiVO$_4$/TiO$_2$/Ti film was successfully fabricated by electrodepositing a nanoporous BiOI film on nanoporous TiO$_2$ arrays followed by annealing at 450°C for 2 h. The electrodeposition of BiOI film was carried out at different times (10, 30, 100, 500 and 1000 s) in Bi(NO$_3$)$_3$ and KI solution. The morphological, crystallographic and photoelectrochemical properties of the prepared BiVO$_4$/TiO$_2$/Ti heterojunction film were examined by using different characterization techniques. UV–vis spectrum absorption studies confirmed an increase in absorption intensities with increasing electrodeposition time, and the band gap of BiVO$_4$/TiO$_2$/Ti film is lower than that of TiO$_2$/Ti. The photocatalytic efficiency of BiVO$_4$/TiO$_2$/Ti heterojunction film was higher compared to that of the TiO$_2$/Ti film owing to the longer transient decay time for BiVO$_4$/TiO$_2$/Ti film (3.2 s) than that of TiO$_2$/Ti film (0.95 s) in our experiment. The BiVO$_4$/TiO$_2$/Ti heterojunction film prepared by electrodeposition for 1000 s followed by annealing showed a high photocurrent density of 0.3363 mA cm^{-2} at 0.6 V versus saturated calomel electrode. Furthermore, the lowest charge transfer resistance from electrochemical impedance spectroscopy was recorded for the BiVO$_4$/TiO$_2$/Ti film (1000 s) under irradiation.

1. Introduction

In the past few decades, photoelectrochemical (PEC) catalytic water splitting by using nanostructured semiconductors has been an effective way of producing hydrogen and oxygen [1,2].

Many types of photoelectrode materials have been reported, including $BiVO_4$, CuO and Fe_3O_4 [3–6]. Among these materials, $BiVO_4$ has attracted significant attention because of its high photocatalytic activity in oxygen evolution under an external bias. However, the conduction band (CB) level is low and it is unsuitable for O_2 formation. The high-energy electrons excited by light usually relax in the bottom of the CB quickly owing to its weak charge-carrier separation [7,8].

Recently, there are two types of modification methods to further improve the photocatalytic ability of the semiconductor photocatalyst of $BiVO_4$. One is doping modification, such as doped metal [9], non-metal [10] and semiconductor [11]. The second method is morphology modification by changing the crystal structure, morphology and specific surface area of $BiVO_4$ [12,13]. The heterogeneous catalytic materials combining with $BiVO_4$ are the most promising structures owing to their uniqueness and excellent coupling ability. There are many types of heterogeneous materials including $WO_3/BiVO_4$, $g-C_3N_4/BiVO_4$ and $TiO_2/BiVO_4$ [14,15].

Among these heterogeneous materials, $BiVO_4/TiO_2$ remains one of the best photocatalytic materials because of the low cost of TiO_2 and the faster electron transfer properties. Moreover, the TiO_2 membrane has great potential in developing highly efficient water treatment and reuse systems, such as the decomposition of organic pollutants [16]. Concerning $BiVO_4/TiO_2$, it has been extensively reported for photo-oxidative degradation of pollutants, such as rhodamine [17,18]. In addition, most of the $BiVO_4/TiO_2$ electrodes are prepared through sol–gel, metal organic decomposition, chemical thermal deposition and spinning [17,19–21]. An efficient charge transfer between $BiVO_4$ and TiO_2 has already been reported [22]. Nanoporous TiO_2/Ti arrays have been successfully prepared by anodic oxidation and the electrocatalytic properties have also been extensively analysed [23]. However, few studies that put porous $BiVO_4$ film onto nanoporous TiO_2/Ti arrays through electrodeposition of BiOI film followed by a sintering method have been conducted.

Therefore, the present work adds useful information on heterogeneous materials. $BiVO_4/TiO_2/Ti$ photoanodes were fabricated by electrodepositing BiOI film on nanoporous TiO_2 arrays followed by annealing at 450°C. PEC characterization of $BiVO_4/TiO_2/Ti$ heterojunction material with different $BiVO_4$ thicknesses was first performed in 0.2 M Na_2SO_4 electrolyte under an Xe lamp irradiation using CHI660E, which will provide new insights on further works in the field of $BiVO_4$-based heterogeneous materials.

2. Experimental procedure

2.1. Preparation of nanoporous TiO_2/Ti film

Commercially pure titanium plates (0.5 mm thick, purity greater than 99.5%) were first degreased in acetone, mechanically polished, and finally, chemically polished at 25°C in a solution consisting of $H_2O : HNO_3 : HF = 6 : 3 : 1$ (vol%) for 30 s. The pretreated titanium plates were anodically oxidized at 25°C in 1 wt% hydrofluoric acid at 20 V for 15 min to produce nanoporous TiO_2/Ti arrays. Then the nanoporous TiO_2 arrays were washed three times with de-ionized water and dried for the next step usage. The prepared nanoporous TiO_2 arrays were sintered in air at 450°C for 2 h to prepare the nanoporous TiO_2/Ti film.

2.2. Preparation of $BiVO_4/TiO_2/Ti$ heterojunction photoanodes

The BiOI film was successfully prepared by electrodeposition [24,25]. The 0.04 M $Bi(NO_3)_3$ solution was prepared by dissolving $Bi(NO_3)_3 \cdot 5H_2O$ in 50 ml 0.4 M KI solution after its pH was adjusted to 2.0 by adding HNO_3. Then the solution was mixed with 20 ml absolute ethanol (100%) containing 0.23 M p-benzoquinone and was vigorously stirred for 15 min. A typical three-electrode cell was used for electrodeposition. Nanoporous TiO_2/Ti film, saturated calomel electrode (SCE) and Pt silk were used as the working electrode, reference electrode and counter electrode, respectively. CHI660E (Shanghai Chenhua Device Company, China) was used for electrodeposition and subsequent PEC studies. Electrodeposition was performed potentiostatically at −0.15 V versus SCE at room temperature with varying deposition times (10, 30, 100, 500 and 1000 s). Then the 0.2 M vanadyl acetylacetonate (VO(acac)$_2$) dissolved in dimethyl sulfoxide was drop-cast onto the working electrode with a volume of 1 ml followed by heating in a muffle furnace at 450°C for 2 h in air. After that, the excess V_2O_5 on the $BiVO_4/TiO_2/Ti$ photoelectrodes was removed in 1 M NaOH solution for 1–2 h with stirring [24].

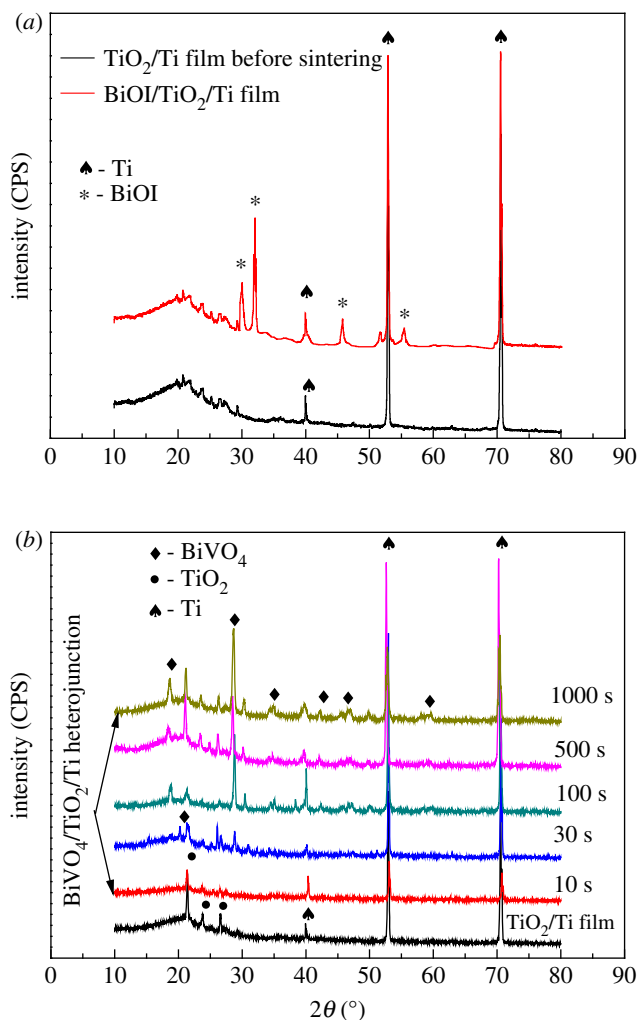**Figure 1.** XRD patterns: (*a*) TiO$_2$/Ti before sintering and BiOI/TiO$_2$/Ti with 1000 s electrodeposition time; (*b*) sintered nanoporous TiO$_2$/Ti film and BiVO$_4$/TiO$_2$/Ti heterojunction films prepared with different electrodeposition times.

The resulting heterojunction BiVO$_4$/TiO$_2$/Ti photoelectrodes were then rinsed with de-ionized water and dried at room temperature.

2.3. Characterization

The surface morphologies of heterojunction BiVO$_4$/TiO$_2$/Ti photoanodes were observed by Hitachi S-4700 field emission scanning electron microscopy (FESEM) after spraying the conducting layer with platinum. The bulk composition was investigated by energy-dispersive X-ray spectroscopy. The phases present in the coatings were characterized by a small angle diffractometric study carried out on a Riga KuD/max 2550PC X-ray automatic diffractometer. The optical performance of the as-prepared materials was evaluated by using a UV–vis Lambda 750S in a wavelength ranging from 300 to 800 nm.

The PEC performance was evaluated in a three-electrode electrochemical cell with a quartz window to allow illumination. The working electrodes were the sintered nanoporous TiO$_2$/Ti film and BiVO$_4$/TiO$_2$/Ti heterojunction film. SCE and Pt silk were used as the reference electrode and counter electrode, respectively. All the working electrodes were characterized in 0.2 M Na$_2$SO$_4$ by CHI660E. Linear sweep voltammetry (LSV) was measured at a scanning rate of 0.01 V s^{-1}. Electrochemical impedance spectroscopy (EIS) was carried out under an open circuit voltage with frequencies ranging from 10^5 to 10^{-2} Hz with an AC voltage amplitude of 5 mV. The potentials in the I–V curves and in the PEC performance experiments were also controlled by CHI660E. A 150 W Xe lamp (Beijing Trust Tech Co. Ltd) was used to provide the visible light. EIS was used to explore the conductivity of the as-compared electrodes in dark and illumination environments in 0.2 M Na$_2$SO$_4$ solution.
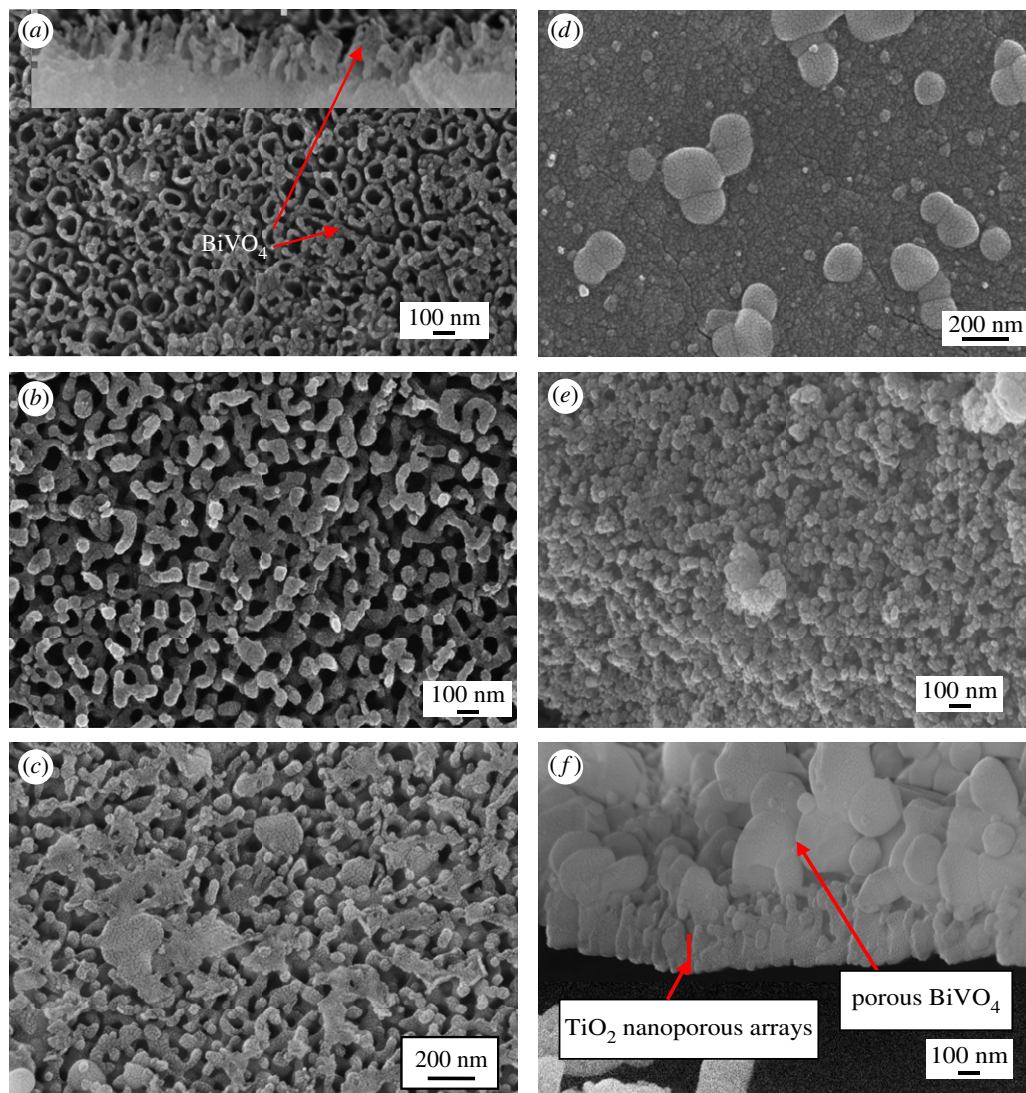
Figure 2. SEM images of photoelectrodes prepared with different electrodeposition times: (*a*) surface image of electrode with 10 s electrodeposition time; inset picture is the cross-section morphology prepared by mechanical fracturing; (*b*) surface image of electrode with 30 s electrodeposition time; (*c*) surface image of electrode with 100 s electrodeposition time; (*d*) surface image of electrode with 500 s electrodeposition time; (*e*) surface image of electrode with 1000 s electrodeposition time; (*f*) cross-section of sample (*e*) with mechanical fracturing.

3. Results and discussion

The crystal structures of sintered nanoporous TiO_2/Ti film and $BiVO_4/TiO_2/Ti$ heterojunction films prepared with different electrodeposition times were characterized by X-ray diffraction (XRD) and are shown in figure 1. In figure 1*a*, the diffraction peaks at 2θ of $29.6°$, $31.6°$, $45.3°$ and $51.3°$ can be indexed to BiOI (JCPDS no. 10–0445). The as-anodized nanoporous TiO_2/Ti films are of amorphous state due to the broad peak and only the peaks of the titanium substrate are present in the diffractogram [26]. After sintering at $450°C$ for 2 h, peaks at approximately $25°$ appear corresponding to anatase phase [26]. After modifying by $BiVO_4$ layer, new peaks appear at 2θ of $18.6°$, $18.9°$, $28.7°$, $34.4°$, $35.2°$, $42.3°$, $46.4°$ and $58.3°$, which correspond to (101), (011), (-121), (200), (002), (051), (002), (202) and (321) of $BiVO_4$. The observed diffraction peaks are in conformity with monoclinic scheelite structure (JCPDS 14-0688). The XRD patterns confirm the full conversion of BiOI to $BiVO_4$ after annealing at $450°C$. From the XRD pattern, it was clarified that $BiVO_4$ could be successfully modified on nanoporous TiO_2/Ti films.

The morphology and nanostructures of $BiVO_4/TiO_2/Ti$ heterojunction photoanodes were characterized using FESEM. Here, the morphology of TiO_2/Ti film was not shown, because its morphology could be easily seen from the morphology of $BiVO_4/TiO_2/Ti$ heterojunction photoanodes

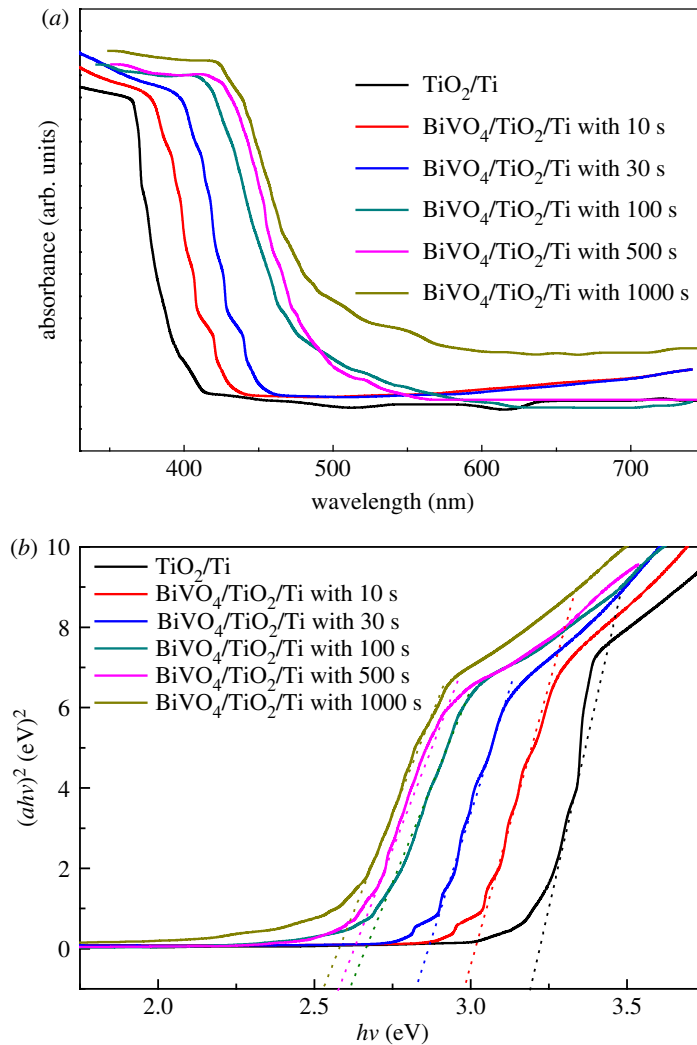**Figure 3.** (a) UV–vis absorption spectra and (b) Tauc plot of nanoporous TiO_2/Ti film and $BiVO_4$/TiO_2/Ti heterojunction films prepared with different electrodeposition times.

obtained with 10 s electrodeposition time. From the top view of the anode with 10 s electrodeposition time (figure 2a), it is found that a small amount of $BiVO_4$ existed in the interstice between the TiO_2 nanotubes and on the top of TiO_2 nanoporous wall. This is confirmed by the cross-section image in the inset picture of figure 2a. The TiO_2 nanotube arrays are formed with regular and orderly structure. The ratio of pore length to diameter was approximately 2 : 1. When the electrodeposition time increased to 30 s, $BiVO_4$ covered the interstices between the TiO_2 walls and left the TiO_2 pores open. Some of the TiO_2 nanopores were covered by $BiVO_4$ when the electrodeposition time increased to 100 s (figure 2c). $BiVO_4$ covered the TiO_2 nanopores and particles of approximately 200 nm grew on the surface when the electrodeposition time increased to 500 s (figure 2d). When the electrodeposition time increased to 1000 s, the morphology of the obtained photoanode was nanoporous and the thickness of $BiVO_4$ was approximately 1 μm. Compared with figure 2d,f, the particle size of $BiVO_4$ is almost 100 nm. This phenomenon is different from the conventional electrodeposition procedure in which the particle size usually increases with electrodeposition time [27].

The UV–vis spectra of TiO_2/Ti film and $BiVO_4$/TiO_2/Ti heterojunction films with different amounts (denoted by the electrodeposition time) of $BiVO_4$ are shown in figure 3a. The absorption edge of the annealed TiO_2/Ti film is approximately 375 nm. After being coupled with $BiVO_4$, the absorption in the visible light region between 400 and 500 nm of $BiVO_4$/TiO_2/Ti heterojunction film increases with the increase in the amount of $BiVO_4$, and the absorption edge shifts to 450 nm for the $BiVO_4$/TiO_2/Ti film prepared with 1000 s electrodeposition time. The band gap of a semiconductor can be calculated by employing the following equation [28]:
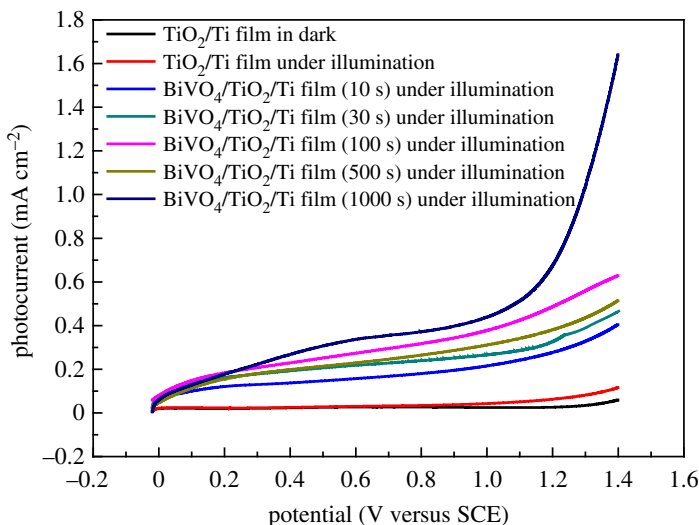
$$(ahv)^2 = hv - E_g, \tag{3.1}$$

Figure 4. LSV plots of nanoporous TiO_2/Ti film and nanoporous $BiVO_4/TiO_2/Ti$ films prepared with different electrodeposition times in 0.2 M Na_2SO_4 solution under 150 W Xe lamp illumination.

where a is the absorption coefficient, v is the light frequency and E_g is the band gap of a semiconductor. From the curve of $(ahv)^2$ versus hv shown in figure 3b, the energy of the band gap of TiO_2/Ti film is 3.20 eV, which is the same as the result reported before [29]. The band gap energies of the $BiVO_4/TiO_2/Ti$ film with 10, 30, 100, 500 and 1000 s electrodeposition times are calculated as 2.98, 2.83, 2.62, 2.58 and 2.53 eV, respectively. All $BiVO_4/TiO_2/Ti$ films exhibited visible-light-driven absorption characteristics. Moreover, the nanoporous $BiVO_4$ film in the $BiVO_4/TiO_2/Ti$ film has slightly shifted on the absorption edge to the larger wavelength within the visible-light range owing to the effect of additional $BiVO_4$.

Figure 4 shows the current–potential plots of nanoporous TiO_2/Ti film and nanoporous $BiVO_4/TiO_2/Ti$ heterojunction photoanodes under a 150 W Xe lamp illumination. The photocurrent densities of nanoporous TiO_2/Ti film in the dark and under illumination were 0.02634 mA cm^{-2} and 0.0308 mA cm^{-2} at 0.6 V (versus SCE), respectively. The $BiVO_4/TiO_2/Ti$ prepared with 10 s electrodeposition time under illumination exhibited a higher photocurrent density of 0.1583 mA cm^{-2} at 0.6 V (versus SCE) and showed a 403% higher photoactivity compared with bare TiO_2/Ti film. Moreover, the photocurrent density of $BiVO_4/TiO_2/Ti$ heterojunction photoanode increased with the increase in electrodeposition time in our experiment. When the electrodeposition time increased to 1000 s, the photocurrent density increased to 0.3363 mA cm^{-2} at 0.6 V (versus SCE). These results clearly indicate that the modification of nanoporous TiO_2/Ti film with $BiVO_4$ effectively reduces the recombination of electrons and holes generated in the nanoporous $BiVO_4/TiO_2/Ti$ film due to the formation of the heterojunction and excellent electron transport between TiO_2 film and the titanium substrate [30]. When $BiVO_4$ layers were coated on the TiO_2 surface, the light absorption range and intensity of $BiVO_4/TiO_2/Ti$ films were improved and the electrons of $BiVO_4$ film could easily transfer to the nanoporous TiO_2, resulting in a high photocurrent density.

The photocurrent response of photoanodes in the electrolyte directly correlates with the generation and transfer of the photo-excited charge carriers in the photocatalytic process [31]. The photocurrent responses of TiO_2/Ti film and $BiVO_4/TiO_2/Ti$ heterojunction films prepared with different electrodeposition times were investigated to enhance the charge separation in 0.2 M Na_2SO_4 electrolyte at 0.6 V bias versus SCE. Both TiO_2 and $BiVO_4$ absorbed the photons and generated electron-hole pairs under the simulated sunlight illumination [32]. As shown in figure 5, it is clear that the photocurrent abruptly increased and decreased when the light source was switched on and off. The photoanodes of $BiVO_4/TiO_2/Ti$ heterojunction films present obviously enhanced the photocurrent response compared with those of bare TiO_2/Ti film. A photocurrent spike is clearly obtained in sudden illumination due to capacitive charging of the interface, and the spike decays because of recombination of the charge carriers associated with holes getting trapped at the surface [33]. When the simulated sunlight was turned on, the photocurrent density was a little higher than that 10 s later, which indicated the poor recombination abilities of photogenerated electrons with the holes in the TiO_2 modified with $BiVO_4$ electrodes [34]. It is obvious that the $BiVO_4/TiO_2/Ti$ heterojunction films
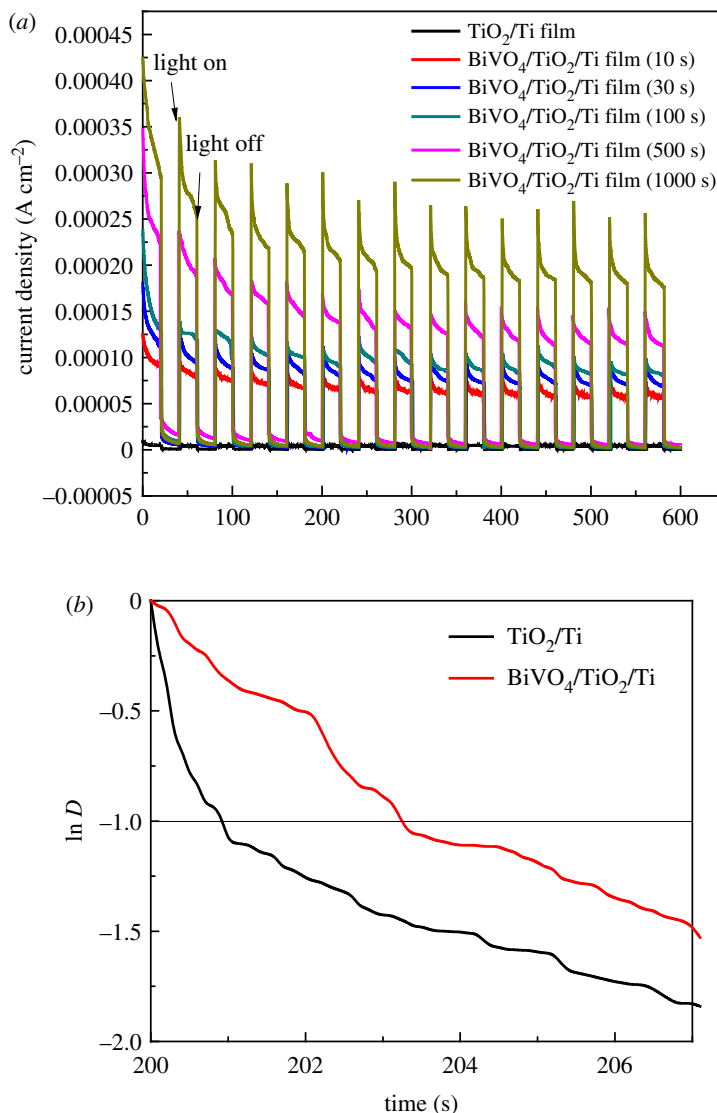
Figure 5. (a) Transient photocurrent responses of TiO_2/Ti film and $BiVO_4/TiO_2/Ti$ heterojunction film prepared with different electrodeposition times under 150 W Xe lamp illumination in 0.2 M Na_2SO_4 solution at 0.6 V versus SCE. (b) Transient decay times of TiO_2/Ti film and $BiVO_4/TiO_2/Ti$ heterojunction film.

with 1000 s electrodeposition time represent the highest photocurrent density compared to that of other photoanodes, which can be ascribed to the high nanoporous surface of $BiVO_4/TiO_2/Ti$ heterojunction photoanodes and their excellent charge separation and transport properties. Thus, it can also be confirmed that the separation of electron-hole pairs was derived from the heterojunction [35].

The transient decay time can be analysed by a logarithmic plot of parameter D, using the following equation [33,36]:

$$D = \frac{I_t - I_s}{I_m - I_s},$$

(3.2)

where I_t is the current at time t, I_s the stabilized current and I_m is the current spike. The transient decay time can be defined as the time at which $\ln D = -1$ [37]. Figure 5b displays the logarithmic plots of parameter D of the $BiVO_4/TiO_2/Ti$ heterojunction film prepared with 10 s and TiO_2/Ti photoelectrodes. The transient decay time for $BiVO_4/TiO_2/Ti$ (3.2 s) is longer than that of TiO_2/Ti (0.95 s), indicating a lower charge carrier recombination rate in $BiVO_4/TiO_2/Ti$ heterojunction photoanodes, leading to an enhanced charge separation efficiency and prolonging the hole lifetimes. The $BiVO_4/TiO_2/Ti$ electrodes prepared with increasing electrodeposition time maintained an improving PEC performance.
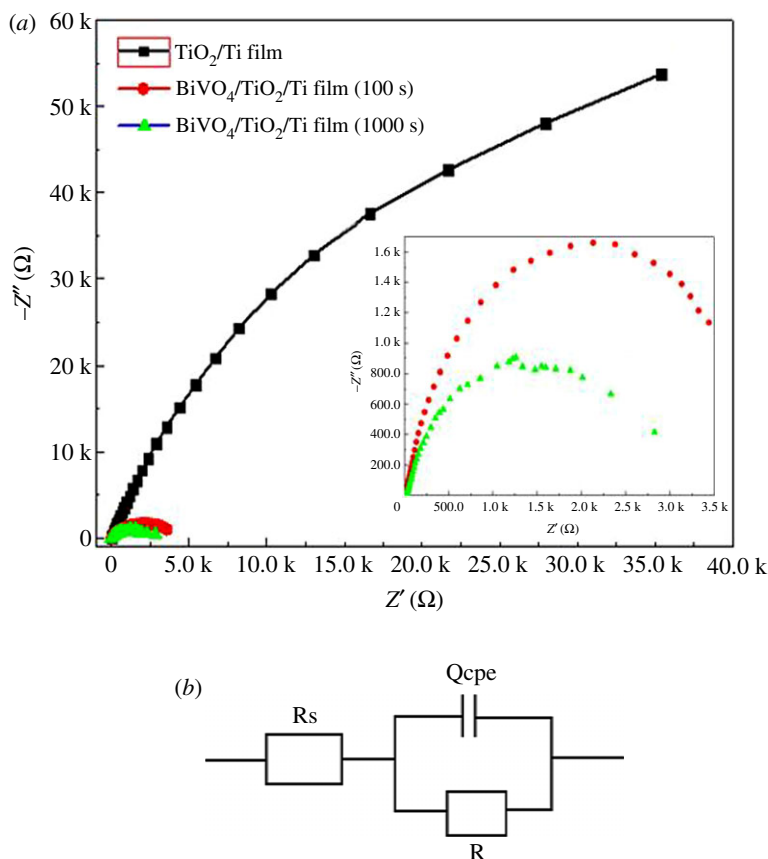
Figure 6. (a) EIS spectra of TiO_2/Ti film and $BiVO_4/TiO_2/Ti$ heterojunction film prepared with different electrodeposition times under 150 W Xe lamp illumination in 0.2 M Na_2SO_4 solution at 0.6 V versus SCE. (b) Equivalent circuit for photoanodes.

To evaluate the kinetics of the charge transfer process of the TiO_2/Ti and $BiVO_4/TiO_2/Ti$ photoelectrodes, EIS tests were carried out at 0.2 V versus SCE under a simulated solar light illumination. Figure 6a displays the Nyquist diagrams in the frequency range of 0.01 Hz to 100 kHz. In the plot, symbols indicate the experimental results and the inset picture is the magnified view of the Nyquist diagram of $BiVO_4/TiO_2/Ti$ heterogeneous photoanodes. The arc in the Nyquist plot indicates the charge transfer kinetics on the working electrode. Obviously, the $BiVO_4/TiO_2/Ti$ photoelectrodes present a lower charge transfer resistance, suggesting that the $BiVO_4/TiO_2/Ti$ heterojunction facilitates charge transfer and separation. The simulated EIS results were obtained from the fitting procedures according to the ZSimpWin software, and the equivalent Randles circuit is shown in figure 6b. In the equivalent Randles circuit, Rs is the solution resistance, Qcpe is the constant phase element for the electrolyte/electrode interface and R is the charge transfer resistance across the interface of electrode/electrolyte. The arcs in the Nyquist plot are related to the charge transfer at the interface of the photoelectrode/electrolyte. The fitted values of R were 3183, 4373 and 322 000 Ω cm^{-2} for $BiVO_4/TiO_2/Ti$ (1000 s), $BiVO_4/TiO_2/Ti$ (100 s) and TiO_2/Ti electrodes, respectively. The efficient charge transfer at the interface between photoelectrode and electrolyte hinders the charge recombination and induces the facile charge transport of electrons through the films. Thus, the bare TiO_2/Ti film has a very low efficiency of charge transfer and shows the highest R value. The lowest R value for $BiVO_4/TiO_2/Ti$ (1000 s) indicates that the charge transfer characteristics of $BiVO_4/TiO_2/Ti$ heterojunction are good. Therefore, the modification of TiO_2/Ti film with nanoporous $BiVO_4$ by forming the heterojunction could improve the charge transfer and photocatalytic ability of photoanodes.

The photogenerated electrons can move to the CB of TiO_2 from the CB of $BiVO_4$ easily owing to the type II heterojunction. The excited electrons in TiO_2 were facilely transported by the conductive Ti and directed to the Pt counter electrode via the external circuit (shown in figure 7). Therefore, the photogenerated electrons were scavenged by hydrogen ions on the Pt foil, while the photogenerated holes oxidized the water on the surface of the $BiVO_4/TiO_2/Ti$. The significantly enhanced PEC performance is attributed to the nanoporous structure, which improved the charge transport [38] and
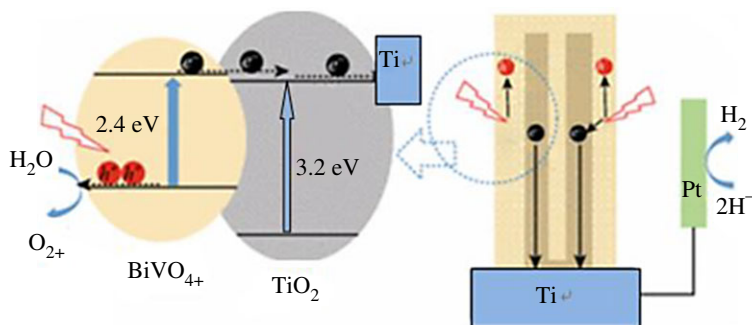
Figure 7. Schematic of energy bands and charge transfers at $BiVO_4/TiO_2/Ti$ film.

collection efficiency as well as the excellent contact between the TiO_2 and $BiVO_4$ with a large interface area facilitating the charge separation. Overall, the $BiVO_4/TiO_2/Ti$ heterojunction film offered a remarkable photoconversion efficiency.

4. Conclusion

A new type of nanoporous $BiVO_4/TiO_2/Ti$ heterojunction photoanode was designed and fabricated by electrodepositing BiOI onto a TiO_2/Ti nanoporous film followed by sintering at $450°C$ in vanadium (IV) oxy acetylacetonate solution for 2 h. A significant change was observed in the PEC properties of the $BiVO_4/TiO_2/Ti$ heterojunction film by varying the electrodeposition time. The film electrodeposited for 1000 s showed a high photocurrent density of $0.3363 \, mA \, cm^{-2}$ at 0.6 V versus SCE. Furthermore, the lowest charge transfer resistance from electrochemical impedance spectroscopy was recorded for the $BiVO_4/TiO_2/Ti$ heterojunction film electrodeposited for 1000 s under irradiation. Our results demonstrate that the nanoporous heterojunction $BiVO_4/TiO_2/Ti$ photoanode is an effective design for improving the PEC performance owing to the excellent transport and separation efficiency. It will open a new opportunity for $BiVO_4/TiO_2/Ti$ heterojunction photoelectrodes for water splitting by using solar energy.

References

1. Jaegermann W, Tributsch H. 1988 Interfacial properties of semiconducting transition metal chalcogenides. *Prog. Surf. Sci.* **29**, 1–167. (doi:10.1016/0079-6816(88)90015-9)

2. Yan K, Qiu Y, Xiao S, Gong J, Zhao S, Xu J, Meng X, Yang S, Xu J. 2017 Self-driven hematite-based photoelectrochemical water splitting cells with three-dimensional nanobowl heterojunction and high-photovoltage perovskite solar cells. *Mater. Today Energy* **6**, 128–135. (doi:10.1016/j.mtener.2017.09.006)

3. Sun T, Cui D, Ma Q, Peng X, Yuan L. 2017 Synthesis of BiVO₄/MWCNT/Ag@AgCl composite with enhanced photocatalytic performance. *J. Phys. Chem. Solids* **111**, 190–198. (doi:10.1016/j.jpcs.2017.08.006)

4. Zhang K, Liu Y, Deng J, Xie S, Dai H. 2017 Fe₂O₃/3DOM BiVO₄: High-performance photocatalysts for the visible light-driven degradation of 4-nitrophenol. *Appl. Catal.*
B **202**, 569–579. (doi:10.1016/j.apcatb.2016.09.069)

5. Baek JH, Kim BJ, Han GS, Hwang SW, Kim DR, Cho IS, Jung HS. 2017 BiVO₄/WO₃/SnO₂ double-heterojunction photoanode with enhanced charge separation and visible-transparency for bias-free solar water-splitting with a perovskite solar cell. *ACS Appl. Mater. Interfaces* **9**, 1479–1487. (doi:10.1021/acsami.6b12782)

6. Wang W, Huang X, Wu S, Zhou Y, Wang L, Shi H, Liang Y, Zou B. 2015 Preparation of p–n junction Cu₂O/BiVO₄ heterogeneous nanostructures with enhanced visible-light photocatalytic activity. *Appl. Catal., B* **134–135**, 293–301. (doi:10.1016/j.apcatb.2013.01.013)

7. Zhou L, Yang Y, Zhang J, Rao PM. 2017 Photoanode with enhanced performance achieved by coating BiVO₄ onto ZnO-templated Sb-doped SnO₂ nanotube scaffold. *ACS Appl.*
Mater. Interfaces **9**, 11 356–11 362. (doi:10.1021/acsami.7b01538)

8. Chang X, Wang T, Zhang P, Li A, Gong J, Zhang J. 2015 and Enhanced surface reaction kinetics and charge separation of p–n heterojunction Co₃O₄/BiVO₄ photoanodes. *J. Am. Chem. Soc.* **137**, 8356–8359. (doi:10.1021/jacs.5b04186)

9. Moniz SJ, Zhu J, Tang J. 2014 1D Co-Pi Modified BiVO₄/ZnO junction cascade for efficient photoelectrochemical water cleavage. *Adv. Energy Mater.* **4**, 1301590. (doi:10.1002/aenm.201301590)

10. Ji Y, Cao J, Jiang L, Zhang Y, Yi Z. 2014 G–C₃N₄/BiVO₄ composites with enhanced and stable visible light photocatalytic activity. *J. Alloys Compd.* **590**, 9–14. (doi:10.1016/j.jallcom.2013.12.050)

11. Guo Z, Li P, Che H, Wang G, Wu C, Zhang X, Mu J. 2016 One-dimensional spindle-like BiVO₄/TiO₂ nanofibers heterojunction nanocomposites with enhanced visible light photocatalytic

activity. *Ceram. Int.* **42**, 4517–4525. (doi:10.1016/j.ceramint.2015.11.142)

12. Su J, Guo L, Bao N, Grimes CA. 2011 Nanostructured WO$_3$/BiVO$_4$ heterojunction films for efficient photoelectrochemical water splitting. *Nano Lett.* **11**, 1928–1933. (doi:10.1021/nl2000743)

13. Dong S, Cui Y, Wang Y, Li Y, Hu L, Sun J, Sun J. 2014 Designing three-dimensional acicular sheaf shaped BiVO$_4$/reduced graphene oxide composites for efficient sunlight-driven photocatalytic degradation of dye wastewater. *Chem. Eng. J.* **249**, 102–110. (doi:10.1016/j.cej.2014.03.071)

14. Park Y, McDonald KJ, Choi K-S. 2013 Progress in bismuth vanadate photoanodes for use in solar water oxidation. *Chem. Soc. Rev.* **42**, 2321–2337. (doi:10.1039/C2CS35260E)

15. Kumar SG, Rao KK. 2015 Tungsten-based nanomaterials (WO$_3$ & Bi$_2$WO$_6$): modifications related to charge carrier transfer mechanisms and photocatalytic applications. *Appl. Surf. Sci.* **355**, 939–958. (doi:10.1016/j.apsusc.2015.07.003)

16. Park N-G, Van de Lagemaat J, Frank AJ. 2000 Comparison of dye-sensitized rutile- and anatase-based TiO$_2$ solar cells. *J. Phys. Chem. B* **104**, 8989–8994. (doi:10.1021/jp994365l)

17. Zhu Z, Han Q, Yu D, Sun J, Liu B. 2017 A novel p-n heterojunction of BiVO$_4$/TiO$_2$/GO composite for enhanced visible-light-driven photocatalytic activity. *Mater. Lett.* **209**, 379–383. (doi:10.1016/j.matlet.2017.08.045)

18. Hua Y, Li D, Wang H, Zeng G, Li X, Shao Y. 2015 Role of active oxygen species in the liquid-phase photocatalytic degradation of RhB using BiVO$_4$/TiO$_2$ heterostructure under visible light irradiation. *J. Mole. Catal. A* **408**, 172–178. (doi:10.1016/j.molcata.2015.07.025)

19. Monfor O, Raptis D, Satrapinskyy L, Roch T, Plesch G, Lianos P. 2017 Production of hydrogen by water splitting in a photoelectrochemical cell using a BiVO$_4$/TiO$_2$ layered photoanode. *Electrochim. Acta* **251**, 244–249. (doi:10.1016/j.electacta.2017.08.125)

20. Zhu X et al. 2016 A shuriken-shaped m-BiVO$_4$/{001}–TiO$_2$ heterojunction: synthesis, structure and enhanced visible light photocatalytic activity. *Appl. Catal., A* **521**, 42–49. (doi:10.1016/j.apcata.2015.10.017)

21. Samsudin MF, Sufian S, Mohamed NM, Bashiri R, Wolfe F, Ramli RM. 2018 Enhancement of hydrogen production over screen-printed TiO$_2$/BiVO$_4$ thin film in the photoelectrochemical cells. *Mater. Lett.* **211**, 13–16. (doi:10.1016/j.matlet.2017.09.013)

22. Rettie AJE et al. 2013 Combined charge carrier transport and photoelectrochemical characterization of BiVO$_4$ single crystals: intrinsic behavior of a complex metal oxide. *J. Am. Chem. Soc.* **135**, 11 389–11 396. (doi:10.1021/ja405550k)

23. Mohamed AE, Rohani S. 2011 Modified TiO$_2$ nanotube arrays (TNTAs): progressive strategies towards visible light responsive photoanode, a review. *Energy Environ. Sci.* **4**, 1065–1086. (doi:10.1039/c0ee00488j)

24. McDonald KJ, Choi KS. 2012 A new electrochemical synthesis route for a BiOI electrode and its conversion to a highly efficient porous BiVO$_4$ photoanode for solar water oxidation. *Energy Environ. Sci.* **9**, 8553–8557. (doi:10.1039/c2ee22608a)

25. Kim T, Choi KS. 2014 Nanoporous BiVO$_4$ photoanodes with dual-layer oxygen evolution catalysts for solar water splitting. *Science* **343**, 990–994. (doi:10.1126/science.1246913)

26. Vujancevic J, Bjelajac A, Cirkovic J. BiVO$_4$ structure and photocatalytic properties of sintered TiO$_2$ nanotube arrays. *Sci. Sintering* **50**, 39–51. (doi:10.2298/SOS1801039V)

27. Mahmood A, Tezcan F, Kardaş G. 2017 Photoelectrochemical characteristics of CuO films with different electrodeposition time. *Int. J. Hydrogen Energy* **42**, 23 268–23 275. (doi:10.1016/j.ijhydene.2017.06.003)

28. Munir S, Shah SM, Hussain H, Ali khan R. 2016 Effect of carrier concentration on the optical band gap of TiO$_2$ nanoparticles. *Mater. Des.* **92**, 64–72. (doi:10.1016/j.matdes.2015.12.022)

29. Tenkyong T, Mary JS, Praveen B, Pugazhendhi K, Sharmila DJ, Shyla JM. 2018 Structural modulation and band gap optimisation of electrochemically anodised TiO$_2$ nanotubes. *Mater. Sci. Semicond. Process.* **83**, 150–158. (doi:10.1016/j.mssp.2018.04.032)

30. Xue L, Sun N, Chen F. 2017 Fabrication of a Ti/TiO$_2$/NiO electrode for electrocatalytic nitrite removal. *Colloids Surf. A* **535**, 1–7. (doi:10.1016/j.colsurfa.2017.09.016)

31. Zhang Y, Lu J, Hoffmann M, Wang Q, Cong Y, Wang Q, Jin H. 2015 Synthesis of gC$_3$N$_4$/Bi$_2$O$_3$/TiO$_2$ composite nanotubes: enhanced activity under visible light irradiation and improved photoelectrochemical activity. *RSC Adv.* **5**, 48 983–48 991. (doi:10.1039/C5RA02750K)

32. Meng X, Li Z, Zhang Z. 2017 Pd-nanoparticle-decorated peanut-shaped BiVO$_4$ improved visible light-driven photocatalytic activity comparable to that of TiO$_2$ under UV light. *J. Catal.* **356**, 53–64. (doi:10.1016/j.jcat.2017.09.005)

33. Zhang H, Cheng C. 2017 Three-dimensional FTO/TiO$_2$/BiVO$_4$ composite inverse opals photoanode with excellent photoelectrochemical performance. *ACS Energy Lett.* **2**, 813–821. (doi:10.1021/acsenergylett.7b00060)

34. Li J, Zhou J, Hao H, Li W. 2017 Controlled synthesis of Fe$_2$O$_3$ modified Ag-010BiVO4 heterostructures with enhanced photoelectrochemical activity toward the dye degradation. *Appl. Surf. Sci.* **399**, 1–9. (doi:10.1016/j.apsusc.2016.12.048)

35. Xia L, Bai J, Li J, Zeng Q, Li X, Zhou B. 2016 A highly efficient BiVO$_4$/WO$_3$/W heterojunction photoanode for visible-light responsive dual photoelectrode photocatalytic fuel cell. *Appl. Catal., B* **183**, 224–230. (doi:10.1016/j.apcatb.2015.10.050)

36. Hagfeldt A, Lindstroem H, Soedergren S, Lindquist S-E. 1995 Photoelectrochemical studies of colloidal TiO$_2$ films: the effect of oxygen studied by photocurrent transients. *J. Electroanal. Chem.* **381**, 39–46. (doi:10.1016/0022-0728(94)03622-A)

37. Bell NJ, Ng YH, Du A, Coster H, Smith SC, Amal R. 2011 Understanding the enhancement in photoelectrochemical properties of photocatalytically prepared TiO$_2$-reduced graphene oxide composite. *J. Phys. Chem. C* **115**, 6004–6009. (doi:10.1021/jp1113575)

38. Xiao XH, Chen XX, Xu TT, Li XJ. 2018 High-efficiency visible photocatalytic degradation of methyl orange by silicon nanoporous pillar array. *Mater. Lett.* **211**, 96–99. (doi:10.1016/j.matlet.2017.09.069)

39. Hongxing D, Qiuping L, Yuehui H. 2018 Data from: Preparation of nanoporous BiVO$_4$/TiO$_2$/Ti film through electrodeposition for photoelectrochemical water splitting. Dryad Digital Repository. (doi:10.5061/dryad.d53pg0j)